Available online at www.sciencedirect.com
ScienceDirect
Journal of Sound and Vibration 317 (2008) 591–607
JOURNAL OF SOUND AND VIBRATION
www.elsevier.com/locate/jsvi

Sensitivity analysis and parameter optimization for vibration reduction of undamped multi-ribbed belt drive systems

Zhi-chao Hou[a,*], Yao-xin Lao[a], Qiu-hai Lu[b]

[a]State Key Laboratory of Automotive Safety and Energy, Tsinghua University, Beijing 100084, People's Republic of China
[b]Department of Engineering Mechanics, Tsinghua University, Beijing 100084, People's Republic of China

Received 22 January 2007; received in revised form 24 January 2008; accepted 30 March 2008
Handling Editor: L.G. Tham
Available online 3 June 2008

Abstract

Tensioner is a critical mechanism to ensure a constant tension level within a serpentine belt drive that is widely used in modern passenger vehicles. For a belt drive with n pulleys, generic and explicit formulae about sensitivities of both frequency and steady harmonic responses are established in terms of system matrices with respect to any design parameter of the system. Deductions from the formulae results in frequency and steady response sensitivities relative to key tensioner parameters and the belt speed. Based on sensitivity analysis, optimizations are conducted on tensioner so as to suppress dynamic responses of the system by frequency detuning. A new approach for searching optimal parameters is put forward by incorporating sensitivity information into a classical coordinate alternating procedure. Examples are given to validate the analytical formulae of the frequency sensitivity and to demonstrate the effect of optimization.

1. Introduction

A serpentine belt drive is widely used to power all front accessories of the engine in modern passenger vehicles. In order to keep a constant tension level in the belt, an automatic belt tensioner is usually adopted, which consists of a tensioner pulley, a tensioner arm and a torsional spring. Although a belt drive is much quieter compared with other drives such as gear drives and so on, evident vibration might occur at certain engine speed due to torque fluctuation from the crankshaft.

Typical vibrations can be roughly classified into three categories. The first category is rotational vibration of the pulleys and tensioner arm around corresponding shafts, where the belt spans act as axial springs [1,2]. The second one is transverse oscillation of belt spans with various boundary conditions supplied by the pulleys and the tensioner [3,4]. Lateral vibration of the belt spans is the third class [5]. It should be pointed out that vibrations of different categories might couple with each other under some circumstances, especially between rotational vibration of pulleys and transverse vibration of belt spans [6,7].

*Corresponding author.
E-mail address: houzc@mail.tsinghua.edu.cn (Z.-c. Hou).

0022-460X/$ - see front matter © 2008 Elsevier Ltd. All rights reserved.
doi:10.1016/j.jsv.2008.03.063

Being able to capture the coupling between rotational and transversal vibrations and thus more accurately describe the actual dynamics of the system, hybrid models have become popular for dynamic analysis on front-end accessory belt drive. A typical hybrid model consists of both discrete variables for the dynamic behavior of pulleys and the tensioner arm, and continuous variables for the transverse dynamics of the belt spans.

For a model belt drive with two pulleys and a tensioner, which was decomposed to an independent belt span and a hybrid subsystem, a Holzer approach with two iteration loops was put forward by Beikmann to calculate the natural frequencies of the hybrid subsystem [6]. Zhang and Zu adopted this prototypical model and derived an explicit equation of frequency for free vibration analysis [7]. Starting from the explicit frequency equation presented in Ref. [7] for the model belt drive, a governing equation on frequency sensitivity with respect to the tensioner parameters was derived by the present authors [8]. The equation was then numerically solved for frequency sensitivity relative to some key design parameters. The approach was validated by results from directly applying a finite difference method to frequency-parameter results obtained by means of the Holzer approach.

It is obvious that the explicit characteristic equation varies with belt configuration and has to be derived case by case. Realizing the demerit, Parker [9] put forward a new method for eigensolution to the hybrid model by introducing Lagrange multipliers to a model of belt drives of n pulleys, where the belt spans adjacent to the tensioner were discretized. Sensitivity analysis of the frequency was also conducted with respect to various design parameters by means of a perturbation method.

The limitation of methods based on the explicit characteristic equation also motivates the present work. For a belt drive with n pulleys, generic and explicit formulae about sensitivities of both frequency and steady harmonic response are established in terms of system matrices with respect to any design parameter of the system. Deductions from the formulae results in frequency and steady response sensitivities relative to key tensioner parameters and the belt speed. Based on sensitivity analysis, optimizations are conducted on tensioner so as to suppress dynamic response of the system. A new approach for searching optimal parameters is put forward by combining a classical procedure and sensitivity analysis. Examples are given to, respectively, validate the analytical formulae of the frequency sensitivity and to demonstrate the effect of optimization.

2. Modeling and equations of motion

2.1. Model and assumptions

For a practical belt drive, the initial tension is usually far less than the tensile stiffness of the belt, i.e. $P_{0i} \ll EA$. The longitudinal wave speed is much faster than the transverse wave speeds corresponding to lower order transverse vibrations. In addition, belt-pulley wedging and slip are not taken into consideration for free vibration analysis of a belt drive under normal operation and small belt motions. Furthermore, in quite a few researches, the flexural stiffness of the belt is neglected and the belt speed is regarded as constant.

The above assumptions are also adopted in this paper, which render the belt to behave pseudo-statically. As a sequel, the mass and stiffness of the belt are uniformly distributed and do not change during operation and vibration. Furthermore, the damping, which plays an important role for the behavior of the system at quasi-resonant vibration, is neglected for the simplicity of introducing the idea and method. It is also based on the same consideration to assume the belt speed as constant although the actual speed usually varies.

Fig. 1 schematically shows a serpentine belt drive that has n pulleys including the tensioner pulley. The pulleys and belt spans are numbered anti-clockwise, with the crankshaft pulley as the first pulley and the span from pulleys 1 to 2 as the first span, respectively. The tensioner arm is pivoted at one end by a torsional spring with k_r as the stiffness coefficient, and supports at another end pulley j ($j = 2$ in Fig. 1) that is also called as tensioner pulley. The constant translating-speed of the belt is notated as c.

The length of the tensioner arm and the moment of inertia of the arm with respect to the pivot are notated as L and J_t, respectively. For pulley $i (i = 1,2,\ldots,n)$, its radius and the moment of inertia relative to its center are denoted by r_i and J_i.

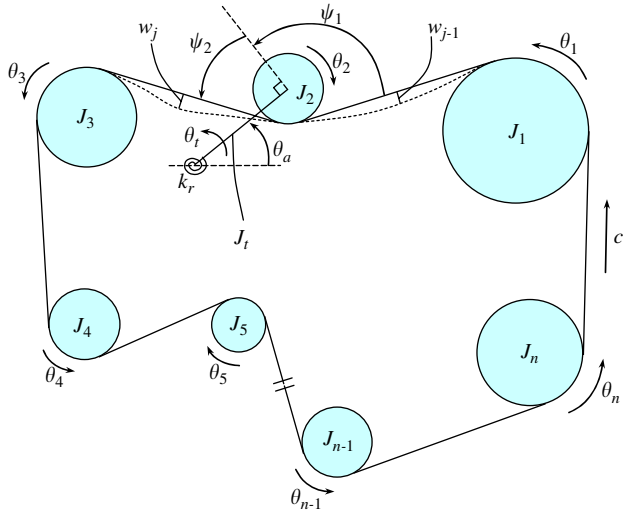

Fig. 1. Schematic of a serpentine belt drive.

The installation angle of the tensioner arm at equilibrium, the rotational angles of the tensioner arm and pulley i relative to the corresponding equilibrium status, are separately represented by θ_a, θ_t and θ_i. Both θ_a and θ_t are positive for an anti-clockwise rotation, while θ_i is positive when the rotation agrees with the translating direction of the belt. The transversal deflection of belt span i is described by w_i, which is positive when the span deforms towards the inner side of the belt drive.

Additionally, two variables, ψ_1 and ψ_2, are defined as shown in Fig. 1, respectively, describe the orientation of the two belt spans adjacent to the tensioner pulley (pulley j). To be more exact, ψ_1 is the angle from belt span $j-1$ to the rotational direction of the tensioner arm, while ψ_2 is the angle from the rotational direction of the arm to belt span j.

2.2. System decomposition

With the above assumptions and understanding, the equations of motion of the belt spans, tensioner arm and pulleys can be derived using Hamilton's principle and Newton's second law, respectively [6–10].

Looking at the linearized equations of all components, it can be observed that only the transverse vibrations of belt spans $j-1$ and j are coupled with the rotational vibration of the tensioner arm and pulleys, but the vibration of all other belt spans is independent. The whole belt drive system can thus be divided into two subsystems as done in literature. The first sub-system consists of $n-2$ independent belt spans. The second subsystem, shown as in Fig. 2, includes all pulleys and the two belt spans adjacent to the tensioner pulley, where other belt spans act as axial springs.

The dynamic characteristics of each belt span within the first subsystem can be readily obtained by directly using the results given by Sacks [11] or Wickert and Mote [12]. In later sections therefore, the first sub-system will not be addressed, but the second sub-system is the focus and will be referred as "system" or "hybrid subsystem" for simplicity.

2.3. Compact equations of free vibration

After the linearized equations of free vibration of all components in the system are obtained, it is assumed that the free vibrations of the pulleys and tensioner arm are harmonic, i.e.

$$\chi_t = \tilde{\chi}_t \cos \omega t, \quad \chi_i = \tilde{\chi}_i \cos \omega t, \quad i = 1, 2, \ldots, n. \tag{1}$$

In the equation, ω is the natural frequency, $\chi_t = L\theta_t$ and $\chi_i = r_i\theta_i$ are the free end displacements of the arm and pulleys due to rotational vibration.

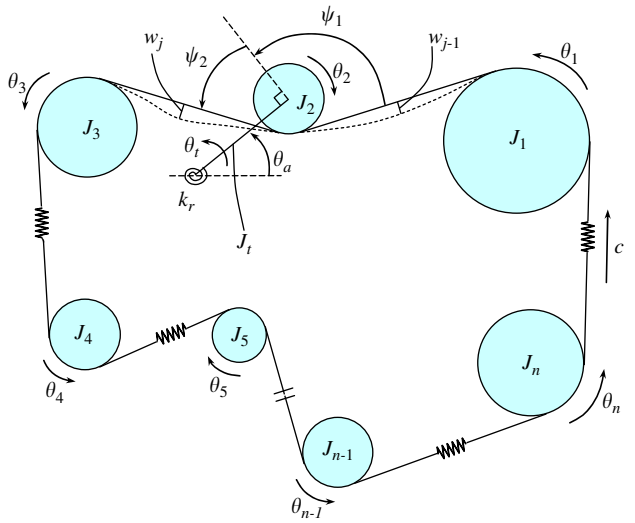

Fig. 2. Sketch of the second sub-system.

Referring to the results of Sack [11] or Wickert and Mote [12], it can be derived for the two belt spans that [7,10]

$$w_{j-1}(x,t) = \frac{-\tilde{\chi}_t \sin\psi_1}{\sin(\omega l_{j-1}/c'_{j-1})} \sin\left(\frac{\omega x}{c'_{j-1}}\right) \cos\left(\omega t + \frac{\omega x - \omega l_{j-1}}{v'_{j-1}}\right), \tag{2}$$

$$w_j(x,t) = \frac{\tilde{\chi}_t \sin\psi_2}{\sin(\omega l_j/c'_j)} \sin\left(\frac{\omega x - \omega l_j}{c'_j}\right) \cos\left(\omega t + \frac{\omega x}{v'_j}\right). \tag{3}$$

Here, c_i' and v_i' are the effective wave speed and phase speed of belt span i ($i = j-1, j$) defined as follows:

$$c'_i = \frac{v_i^2 - c^2}{v_i}, \quad v'_i = \frac{v_i^2 - c^2}{c}, \quad v_i = \sqrt{\frac{P_{0i}}{m}}. \tag{4}$$

Substituting Eqs. (2) and (3) into the equations of the system, and canceling $\cos\omega t$ from each items in the resulting equation, ultimately lead to a compact-formed equation of motion for all discrete components as

$$(\mathbf{K}_D - \omega^2 \mathbf{M}_D)\mathbf{X} = 0 \tag{5}$$

with

$$\mathbf{X} = \begin{bmatrix} \tilde{\chi}_1 & \tilde{\chi}_2 & \cdots & \tilde{\chi}_n & \tilde{\chi}_t \end{bmatrix}^{\mathrm{T}}, \tag{6}$$

$$\mathbf{K}_D = \begin{bmatrix} \mathbf{K}_d & \mathbf{h} \\ \mathbf{h}^{\mathrm{T}} & K_t \end{bmatrix}, \quad \mathbf{M}_D = \begin{bmatrix} \mathbf{M}_d & 0 \\ 0 & m_t \end{bmatrix}. \tag{7}$$

The sub-matrices or entries in Eq. (7) are defined by

$$\mathbf{K}_d = \begin{bmatrix} k_1+k_n & -k_1 & \vdots & 0 & -k_n \\ & k_1+k_2 & \vdots & 0 & 0 \\ & & \ddots & \cdots & \cdots \\ & & & k_{n-2}+k_{n-1} & -k_{n-1} \\ \text{Sym.} & & & & k_{n-1}+k_n \end{bmatrix}, \tag{8}$$

$$\mathbf{M}_d = \begin{bmatrix} m_1 & 0 & 0 & \vdots & 0 & 0 \\ 0 & m_2 & 0 & \vdots & 0 & 0 \\ 0 & 0 & m_3 & \vdots & 0 & 0 \\ \cdots & \cdots & \cdots & \ddots & \cdots & \cdots \\ 0 & 0 & 0 & \vdots & m_{n-1} & 0 \\ 0 & 0 & 0 & \vdots & 0 & m_n \end{bmatrix}, \ \mathbf{h} = \begin{bmatrix} 0 \\ \vdots \\ k_{j-1}\cos\psi_1 \\ -k_{j-1}\cos\psi_1 + k_j\cos\psi_2 \\ -k_j\cos\psi_2 \\ \vdots \\ 0 \end{bmatrix}, \tag{9}$$

$$K_t = P_{t(j-1)}\sin^2\psi_1 \cot\left(\frac{\omega l_{j-1}}{c'_{j-1}}\right)\frac{\omega}{c'_{j-1}} + P_{tj}\sin^2\psi_2 \cot\left(\frac{\omega l_j}{c'_j}\right)\frac{\omega}{c'_j} + k_{j-1}\cos^2\psi_1 + k_j\cos^2\psi_2 + k_s + k_{\mathrm{gr}}, \tag{10}$$

$$m_t = J_t/L^2 + \hat{m}_j. \tag{11}$$

In the above expressions, $P_{ti} = P_{0i} - mc^2$ is the tensile force carried by belt span i at steady status, where P_{0i} is the initial static tension and m is the mass per unit length of the belt. The equivalent mass of pulley i is denoted as $m_i = J_i/r_i^2$, while $\hat{m}_j$ is the mass of the tensioner pulley and other related accessories. The stiffness of belt span i is described by $k_i = \mathrm{EA}/l_i$ with l_i as the span length. Equivalent stiffness $k_s = k_r/L^2$ is a transformed stiffness of the torsional spring, and the geometrical stiffness of the tensioner arm k_{gr} is calculated by

$$k_{\mathrm{gr}} = \frac{P_{t(j-1)}\sin\psi_1 - P_{tj}\sin\psi_2}{L}. \tag{12}$$

It should be noted in Eq. (9) that $(-k_{j-1}\cos\psi_1 + k_j\cos\psi_2)$ is the jth component of vector $\mathbf{h}$. To be more exact, if $j = 1$, $k_{j-1}\cos\psi_1$ is the nth component of the vector. If $j = n$ on the other hand, $-k_j\cos\psi_2$ is the first component.

2.4. Compact equation of forced vibration

When pulley $i(i = 1,2,\ldots,n)$ and tensioner arm are subjected to external moments M_{ei} and M_t, respectively, similar approaches as adopted for free vibration analysis can be used to derive the equations governing the forced vibration of the system [10].

As a tentative trial, all external excitations are assumed to be harmonic, having an identical frequency ω_e and being in phase. Assuming the initial phase angles to be zero without loss of generality, it follows

$$f_{ei} = \tilde{f}_{ei}\cos\omega_e t, \quad f_{et} = \tilde{f}_{et}\cos\omega_e t. \tag{13}$$

Here $f_{ei} = M_{ei}/r_i$, $f_{et} = M_{et}/L$. The steady responses of all discrete components are thus harmonic and can be expressed as

$$\chi_{ri} = \tilde{\chi}_{ri} \cos \omega_e t,\ \chi_{rt} = \tilde{\chi}_{rt} \cos \omega_e t. \tag{14}$$

According to Eqs. (2) and (3), it can be derived that

$$w_{r,(j-1)}(x,t) = \frac{-\tilde{\chi}_{rt} \sin \psi_1}{\sin(\omega_e l_{j-1}/c'_{j-1})} \sin\left(\frac{\omega_e x}{c'_{j-1}}\right) \cos\left(\omega_e t + \frac{\omega_e x - \omega_e l_{j-1}}{v'_{j-1}}\right), \tag{15}$$

$$w_{rj}(x,t) = \frac{\tilde{\chi}_{rt} \sin \psi_2}{\sin(\omega_e l_j/c'_j)} \sin\left(\frac{\omega_e x - \omega_e l_j}{c'_j}\right) \cos\left(\omega_e t + \frac{\omega_e x}{v'_j}\right). \tag{16}$$

Combining together the steady responses of all components under forced vibration finally leads to a compact-formed equation as

$$(\mathbf{K}_D - \omega_e^2 \mathbf{M}_D)\tilde{\mathbf{X}}_r = \tilde{\mathbf{F}}_e, \tag{17}$$

where

$$\tilde{\mathbf{X}}_r = \begin{bmatrix} \tilde{\chi}_{r1} & \tilde{\chi}_{r2} & \cdots & \tilde{\chi}_{rn} & \tilde{\chi}_{rt} \end{bmatrix}^{\mathrm{T}}, \quad \tilde{\mathbf{F}}_e = \begin{bmatrix} \tilde{f}_{e1} & \tilde{f}_{e2} & \cdots & \tilde{f}_{en} & \tilde{f}_{et} \end{bmatrix}^{\mathrm{T}}. \tag{18}$$

With the solutions to Eq. (17), Eq. (14) presents the steady responses of each pulley and the tensioner arm. The expressions of $w_{r,\,(j-1)}(x,\,t)$ and $w_{rj}(x,\,t)$ are obtained by substituting $\tilde{\chi}_{rt}$ into Eqs. (15) and (16), from which two variables are extracted as follows:

$$A_{b,(j-1)} = \frac{-\tilde{\chi}_{rt} \sin \psi_1}{\sin(\omega_e l_{j-1}/c'_{j-1})}, \quad A_{bj} = \frac{\tilde{\chi}_{rt} \sin \psi_2}{\sin(\omega_e l_j/c'_j)}. \tag{19}$$

For concise of description in later sections, each variable is called as amplitude of the corresponding belt span at the forced vibration.

3. Frequency sensitivity

3.1. A generic formula

According to Eq. (5), the normalized modal vector φ_k corresponding to frequency ω_k satisfies

$$(\mathbf{K}_D - \omega_k^2 \mathbf{M}_D)\varphi_k = 0. \tag{20}$$

Differentiating each term in Eq. (20) with respect to design parameter p_m, pre-multiplying the subsequent equation by φ_k^{T}, considering the symmetry of matrices $\mathbf{K}_D$ and $\mathbf{M}_D$, and using Eq. (20) ultimately yield

$$\varphi_k^{\mathrm{T}} \frac{\partial \mathbf{K}_D}{\partial p_m} \varphi_k - 2\omega_k \frac{\partial \omega_k}{\partial p_m} \varphi_k^{\mathrm{T}} \mathbf{M}_D \varphi_k - \omega_k^2 \varphi_k^{\mathrm{T}} \frac{\partial \mathbf{M}_D}{\partial p_m} \varphi_k = 0. \tag{21}$$

Dividing the modal vector φ_k into two sub-sets as $\varphi_k^{\mathrm{T}} = [\,\varphi_{k1}^{\mathrm{T}} \quad \varphi_{k2}^{\mathrm{T}}\,]$ with $\varphi_{k1} = [\,\widehat{\chi}_{r1} \ \ \widehat{\chi}_{r2} \ \ \cdots \ \ \widehat{\chi}_{rn}\,]^{\mathrm{T}}$ and $\varphi_{k2} = \widehat{\chi}_{rt}$, it can then be found that

$$\varphi_k^{\mathrm{T}} \frac{\partial \mathbf{K}_D}{\partial p_m} \varphi_k = \varphi_{k1}^{\mathrm{T}} \frac{\partial \mathbf{K}_d}{\partial p_m} \varphi_{k1} + 2\varphi_{k1}^{\mathrm{T}} \frac{\partial \mathbf{h}}{\partial p_m} \varphi_{k2} + \varphi_{k2}^{\mathrm{T}} \frac{\partial K_t}{\partial p_m} \varphi_{k2}. \tag{22}$$

Recalling Eq. (10), it is observed that K_t is a function of ω_k and p_m. Denoting $K_t = G(\omega_k,\, p_m)$, it follows

$$\frac{\partial K_t}{\partial p_m} = \frac{\partial G}{\partial \omega_k} \frac{\partial \omega_k}{\partial p_m} + \frac{\partial G}{\partial p_m}. \tag{23}$$

Substituting Eq. (22) into Eq. (21) and using Eq. (23), result in an explicit expression on the sensitivity of the natural frequency ω_k with respect to the design parameter p_m,

$$\frac{\partial\omega_k}{\partial p_m}=\left(\varphi_{k1}^{\mathrm{T}}\frac{\partial\mathbf{K}_d}{\partial p_m}\varphi_{k1}+2\varphi_{k1}^{\mathrm{T}}\frac{\partial\mathbf{h}}{\partial p_m}\varphi_{k2}+\varphi_{k2}^{\mathrm{T}}\frac{\partial G}{\partial p_m}\varphi_{k2}-\omega_k^2\varphi_k^{\mathrm{T}}\frac{\partial\mathbf{M}_D}{\partial p_m}\varphi_k\right)\Big/\left(2\omega_k\varphi_k^{\mathrm{T}}\mathbf{M}_D\varphi_k-\varphi_{k2}^{\mathrm{T}}\frac{\partial G}{\partial\omega_k}\varphi_{k2}\right). \tag{24}$$

3.2. Derived expressions

Replacing p_m in Eq. (24) in turn by the installation angle θ_a of the tensioner arm, the arm length L, the stiffness of the torsional spring k_r and the belt speed c, yields in sequence the frequency sensitivities as [10]

$$\frac{\partial\omega_k}{\partial\theta_a}=\frac{\varphi_{k1}^{\mathrm{T}}(\partial\mathbf{K}_d/\partial\theta_a)\varphi_{k1}+2\varphi_{k1}^{\mathrm{T}}(\partial\mathbf{h}/\partial\theta_a)\varphi_{k2}+\varphi_{k2}^{\mathrm{T}}(\partial G/\partial\theta_a)\varphi_{k2}}{2\omega_k\varphi_k^{\mathrm{T}}\mathbf{M}_D\varphi_k-\varphi_{k2}^{\mathrm{T}}(\partial G/\partial\omega_k)\varphi_{k2}}, \tag{25}$$

$$\frac{\partial\omega_k}{\partial L}=\left(\varphi_{k1}^{\mathrm{T}}\frac{\partial\mathbf{K}_d}{\partial L}\varphi_{k1}+2\varphi_{k1}^{\mathrm{T}}\frac{\partial\mathbf{h}}{\partial L}\varphi_{k2}+\varphi_{k2}^{\mathrm{T}}\frac{\partial G}{\partial L}\varphi_{k2}-\omega_k^2\varphi_k^{\mathrm{T}}\frac{\partial\mathbf{M}_D}{\partial L}\varphi_k\right)\Big/\left(2\omega_k\varphi_k^{\mathrm{T}}\mathbf{M}_D\varphi_k-\varphi_{k2}^{\mathrm{T}}\frac{\partial G}{\partial\omega_k}\varphi_{k2}\right), \tag{26}$$

$$\frac{\partial\omega_k}{\partial k_r}=\frac{\varphi_{k2}^{\mathrm{T}}(\partial G/\partial k_r)\varphi_{k2}}{2\omega_k\varphi_k^{\mathrm{T}}\mathbf{M}_D\varphi_k-\varphi_{k2}^{\mathrm{T}}(\partial G/\partial\omega_k)\varphi_{k2}}, \tag{27}$$

$$\frac{\partial\omega_k}{\partial c}=\frac{\varphi_{k2}^{\mathrm{T}}(\partial G/\partial c)\varphi_{k2}}{2\omega_k\varphi_k^{\mathrm{T}}\mathbf{M}_D\varphi_k-\varphi_{k2}^{\mathrm{T}}(\partial G/\partial\omega_k)\varphi_{k2}}. \tag{28}$$

4. Sensitivity of steady harmonic responses

Differentiating Eq. (17) with respect to design parameter p_m, finally yields

$$\frac{\partial\tilde{\mathbf{X}}_r}{\partial p_m}=[\mathbf{K}_D-\omega_e^2\mathbf{M}_D]^{-1}\left(\omega_e^2\frac{\partial\mathbf{M}_D}{\partial p_m}-\frac{\partial\mathbf{K}_D}{\partial p_m}\right)\tilde{\mathbf{X}}_r, \tag{29}$$

where

$$\frac{\partial\tilde{\mathbf{X}}_r}{\partial p_m}=\left[\frac{\partial\tilde{\chi}_{r1}}{\partial p_m}\quad\frac{\partial\tilde{\chi}_{r2}}{\partial p_m}\quad\cdots\frac{\partial\tilde{\chi}_{rn}}{\partial p_m}\quad\frac{\partial\tilde{\chi}_{rt}}{\partial p_m}\right]^{\mathrm{T}}. \tag{30}$$

The expression $(\partial\omega_e/\partial p_m)=0$ is adopted during the derivation, as there is no relation between exciting frequency ω_e and the parameter p_m. From Eqs. (29) and (30), the sensitivity of the amplitude of each discrete component can be readily computed with respect to any design parameter.

According to Eq. (19), the sensitivity of the amplitudes of both belt spans can be obtained from definition relative to the design parameter p_m as

$$\begin{aligned}\frac{\partial A_{b,(j-1)}}{\partial p_m}=&-\frac{\partial\tilde{\chi}_{rt}}{\partial p_m}\frac{\sin\psi_1}{\sin(\omega_e l_{j-1}/c'_{j-1})}-\frac{\tilde{\chi}_{rt}\cos\psi_1}{\sin(\omega_e l_{j-1}/c'_{j-1})}\frac{\mathrm{d}\psi_1}{\mathrm{d}p_m}\\&+\frac{\tilde{\chi}_{rt}\sin\psi_1\cot(\omega_e l_{j-1}/c'_{j-1})}{\sin(\omega_e l_{j-1}/c'_{j-1})}\left(\frac{\omega_e}{c'_{j-1}}\frac{\mathrm{d}l_{j-1}}{\mathrm{d}p_m}-\frac{\omega_e l_{j-1}}{c'^2_{j-1}}\frac{\mathrm{d}c'_{j-1}}{\mathrm{d}p_m}\right),\end{aligned} \tag{31}$$

$$\begin{aligned}\frac{\partial A_{bj}}{\partial p_m}=&\frac{\partial\tilde{\chi}_{rt}}{\partial p_m}\frac{\sin\psi_2}{\sin(\omega_e l_j/c'_j)}+\frac{\tilde{\chi}_{rt}\cos\psi_2}{\sin(\omega_e l_j/c'_j)}\frac{\mathrm{d}\psi_2}{\mathrm{d}p_m}\\&-\frac{\tilde{\chi}_{rt}\sin\psi_2\cot(\omega_e l_j/c'_j)}{\sin(\omega_e l_j/c'_j)}\left(\frac{\omega_e}{c'_j}\frac{\mathrm{d}l_j}{\mathrm{d}p_m}-\frac{\omega_e l_j}{c'^2_j}\frac{\mathrm{d}c'_j}{\mathrm{d}p_m}\right).\end{aligned} \tag{32}$$

The detail expressions of

$$\frac{d\psi_1}{dp_m}, \frac{d\psi_2}{dp_m}, \frac{dl_{j-1}}{dp_m}, \frac{dl_j}{dp_m}, \frac{dc'_{j-1}}{dp_m} \quad \text{and} \quad \frac{dc'_j}{dp_m}$$

can be found from definition and algebraic manipulations [10].

5. Parameter optimization for vibration reduction

5.1. Model for optimization

Low vibration level is always pursued during the design of a belt drive system. Compared with other components, it is easier to adjust the tensioner so as to achieve a better vibration and noise performance. It is thus natural to choose the installation angle of the tensioner arm θ_a, the length of the tensioner arm L and the stiffness of the torsional spring k_r as design variables for optimization. The objective function can then be defined as

$$\begin{cases} \psi = \min \Gamma(\theta_a, L, k_r) \\ \Gamma(\theta_a, L, k_r) = \sum_{i=1}^{n} \mu_i(\tilde{\chi}_{ri})^2 + \mu_t(\tilde{\chi}_{rt})^2 + \mu_{b1}(A_{b,(j-1)})^2 + \mu_{b2}(A_{bj})^2 \cdot \end{cases} \tag{33}$$

Here $\tilde{\chi}_{ri}$, $\tilde{\chi}_{rt}$, $A_{b,(j-1)}$ and A_{bj} are, respectively, the amplitudes of pulley i, the tensioner arm and belt spans as defined before, while μ_i, μ_t, μ_{b1} and μ_{b2} are the corresponding weighting factors.

The requirements of no motion interference and possible stiffness of the torsional spring lead to a set of constraints

$$\begin{cases} \theta_a^L \leqslant \theta_a \leqslant \theta_a^U, \\ L^L \leqslant L \leqslant L^U, \\ k_r^L \leqslant k_r \leqslant k_r^U, \end{cases} \tag{34}$$

where the superscripts L and U represent lower and upper limits, respectively.

5.2. Optimal algorithm

A coordinate alternating (CA) path-searching procedure is used for optimization. Modifications are made by adding additional path-searches and using sensitivity information of the objective function to enhance the robustness and efficiency of the procedure [10].

5.2.1. Sensitivity and extrema of the objective function

From Eq. (33), the sensitivity of function $\Gamma(\theta_a, L, k_r)$ with respect to a design variable $p_m \in (\theta_a, L, k_r)$ can be derived by definition as

$$\frac{d\Gamma(\theta_a, L, k_r)}{dp_m} = \sum_{i=1}^{n} \left(2\mu_i \tilde{\chi}_{ri} \frac{\partial \tilde{\chi}_{ri}}{\partial p_m} \right) + 2\mu_t \tilde{\chi}_{rt} \frac{\partial \tilde{\chi}_{rt}}{\partial p_m} + 2\mu_{b1} A_{b,(j-1)} \frac{\partial A_{b,(j-1)}}{\partial p_m} + 2\mu_{b2} A_{bj} \frac{\partial A_{bj}}{\partial p_m}. \tag{35}$$

The involved sensitivity of the amplitude of each relevant component can be calculated using Eqs. (29), (31) or (32).

The objective function takes a local minimum when the values of the design variables simultaneously satisfy

$$\frac{d\Gamma}{d\theta_a} = 0, \quad \frac{d\Gamma}{dL} = 0, \quad \frac{d\Gamma}{dk_r} = 0 \tag{36}$$

and

$$\frac{d^2\Gamma}{d\theta_a^2} > 0, \quad \frac{d^2\Gamma}{dL^2} > 0, \quad \frac{d^2\Gamma}{dk_r^2} > 0. \tag{37}$$

These values, if exist, are the desired ones of optimization, or at least good initials for later optimization. Due to the limitation on the design variables imposed by the constraints unfortunately, Eqs. (36) and (37) cannot always be satisfied.

When no combination of the design variables satisfies both sets of equations, suboptimal values of the design variables should be pursued. The basic idea is schematically demonstrated in Fig. 3, which presents the two possibilities of a problem with one design variable.

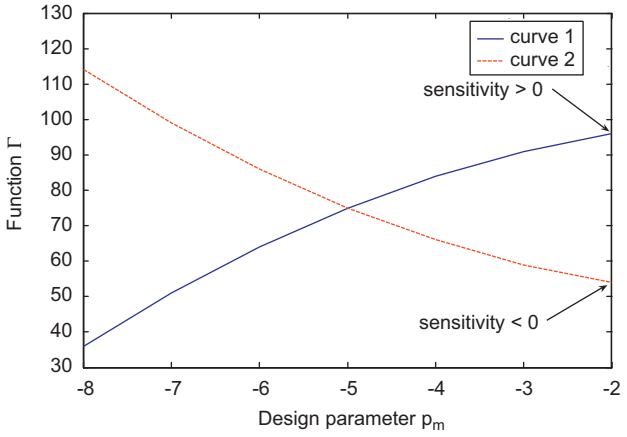

Fig. 3. Extrema on boundary of definition domain.

Suppose that $p_m^{\max}$ is the upper limit of design parameter p_m within certain interval, referring to curve 1 in Fig. 3. If

$$\left.\frac{\partial \Gamma}{\partial p_m}\right|_{p_m=p_m^{\max}} > 0,$$

$\Gamma(p_m^{\max})$ takes the maximum value in the vicinity of $p_m^{\max}$. On the other hand, if

$$\left.\frac{\partial \Gamma}{\partial p_m}\right|_{p_m=p_m^{\max}} < 0,$$

$\Gamma(p_m^{\max})$ takes the minimal value in the vicinity, as shown by curve 2 in the figure. At the lower boundary of p_m, or in the vicinity of $p_m^{\min}$, similar discussions can be made. The calculation and evaluation on both the lower and upper boundaries of a design parameter can be called as boundary analysis.

The bisection method is employed to get the solution to $(\partial \Gamma/\partial p_m) = 0$. If there is not any value of p_m that satisfies this equation due to constraints, boundary analysis will be performed to determine a suboptimal solution for the objective function.

5.2.2. Improved CA procedure

A CA method transfers a path-searching problem of multiple dimensions into a series of one-dimension problems, which is very suitable to optimization problems of a small dimension. With a traditional CA approach, a one-dimensional path-searching is conducted coordinate by coordinate. A complete searching loop is finished once all coordinates have been targeted. The values of design variables resulted from the just finished searching loop are used to start a new round of searching for a better target. The searching procedures will continue until an optimal solution is found.

In order to increase the possibility of finding a global optimal solution, additional searching path should be adopted [10]. This procedure with additional searches is called as improved coordinate alternating (ICA)

method in later sections. The necessity can be explained schematically using a two-dimensional problem as shown in Fig. 4.

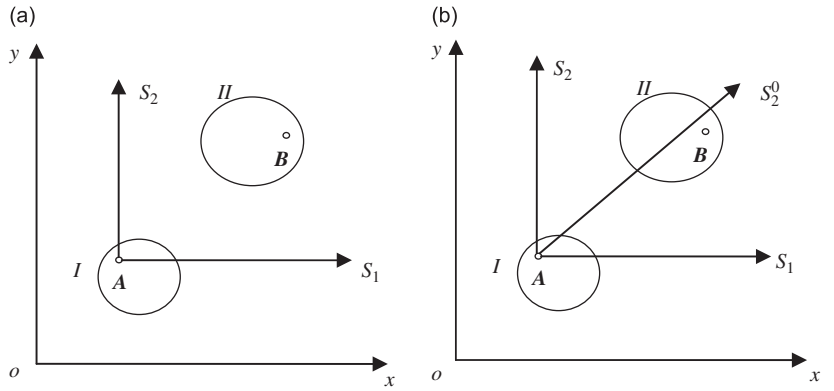

Fig. 4. Qualitative comparison to CA and ICA approaches.

For this two-dimensional problem, point A is assumed to be an optimal solution in the sub-domain I while point B is the global optimal solution. Furthermore, each point within the vicinity of point B or domain II is a better solution than point A to reach point B. As a result of previous path-searching loops, point A is obtained. With a traditional CA method as shown in Fig. 4(a), the next searching loop will be conducted in two directions of S_1 and S_2, respectively. It is obvious that both searches within the loop will unfortunately miss domain II.

In Fig. 4(b), additional searches are used after finishing the search along S_1 but before searching along S_2, notated as $S_2^i (i = 0,1,\ldots,m)$. This way the global optimal, point B, can be found with a higher possibility. The exact number of additional searches, m, can be determined by trial and error with a compromise between resolution and efficiency.

Numerical simulations demonstrated that the optimal solution obtained by ICA process might change with initial values of design variables, although ICA process has a much better robustness in this regard compared with the traditional CA procedure [10]. In order to decrease such dependence, sensitivity information and boundary analysis are incorporated into ICA process to construct a new optimal algorithm, whose flowchart is shown in Fig. 5.

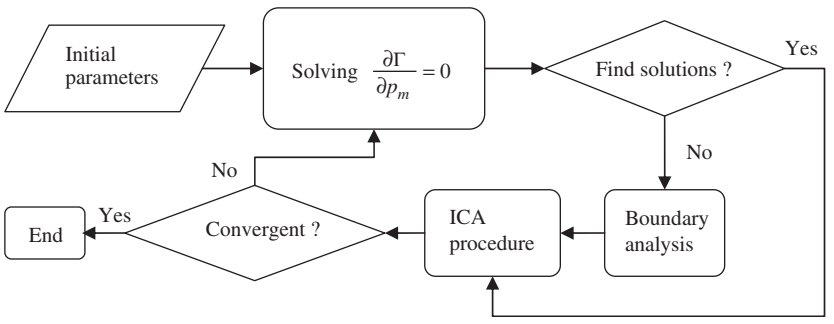

Fig. 5. Flowchart of the optimal procedure.

6. Examples and discussions

Two examples are presented to exemplify the sensitivity analysis and design optimization for vibration reduction. In both examples, the Holzer method is used to calculate the natural frequency of the hybrid subsystem.

6.1. Frequency sensitivity analysis

For the model belt drive introduced in Ref. [6] and shown in Fig. 6, sensitivity analysis of the first natural frequency of the hybrid sub-system is conducted with respect to the installation angle θ_a, arm length L, stiffness of the torsional spring k_r and the translating speed c. Initial values of the design parameters are taken as $\theta_a = -3.75^\circ$, $L = 0.097\,\text{m}$, $k_r = 4.37\,\text{N m/rad}$ and $c = 0\,\text{m/s}$, respectively. The rest parameters are presented in Table 1.

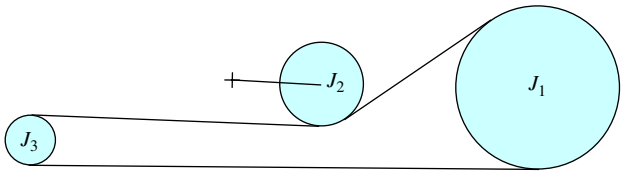

Fig. 6. A model belt drive of three pulleys.

Table 1
Parameters of the model drive of three pulleys

Components	(x, y)[a](m)	r_i/L (m)	J_i/J_t (kg m^2)
Pulley 1	(0.5525, 0.0556)	0.0889	0.07248
Pulley 2	–	0.0452	0.000293
Pulley 3	(0.0, 0.0)	0.02697	0.000293
Tensioner arm	(0.2508, 0.0635)	–	0.001165
EA $= 170,000\,\text{N}$; $m = 0.1029\,\text{kg/m}$; $P_{0i} = 128.7\,\text{N}$; $\hat{m}_j = 0.302\,\text{kg}$			

[a](x, y) are the coordinates of a pulley center or the tensioner arm pivot. Center coordinates of tensioner pulley are calculated according to θ_a and L.

It can be observed clearly from Figs. 7 to 9 that the sensitivity results from explicit formulae derived in this paper agree very well with those predicted by numerically solving the governing equation of sensitivity and another direct numerical method [8].

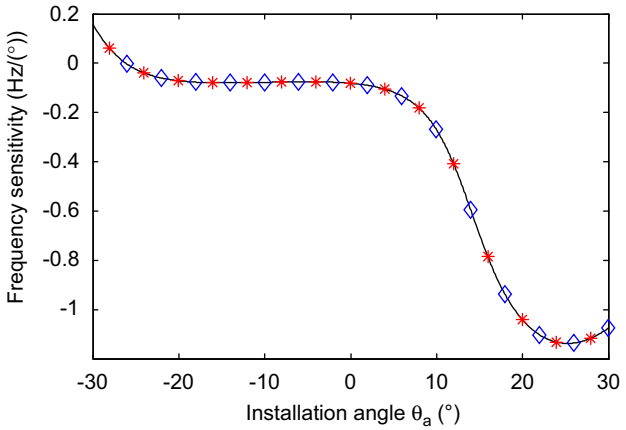

Fig. 7. Sensitivity of ω_1 relative to θ_a. ***, direct numerical method [8]; ◇ ◇ ◇, solution of governing equation [8]; —, explicit formula.

In Fig. 10, the sensitivity of the first ten natural frequencies of the subsystem is depicted with respect to the translating speed. It is noted that the sensitivity of the second frequency, which corresponds to a rotational mode, is almost zero for the whole effective speed range. On the other hand, those frequencies corresponding to

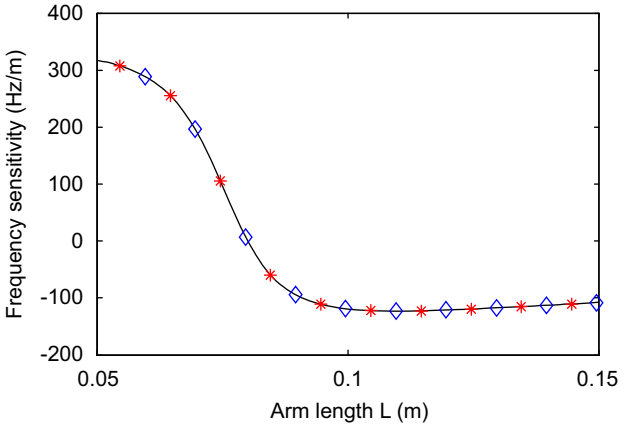

Fig. 8. Sensitivity of ω_1 relative to L. ***, direct numerical method [8]; ◇ ◇ ◇, solution of governing equation [8]; —, explicit formula.

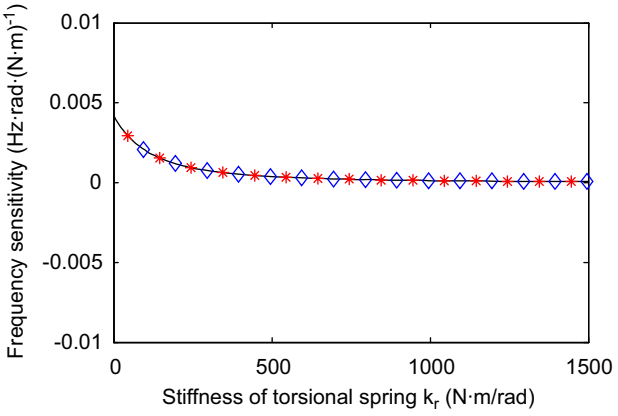

Fig. 9. Sensitivity of ω_1 relative to k_r. ***, direct numerical method [8]; ◇ ◇ ◇, solution of governing equation [8]; —, explicit formula.

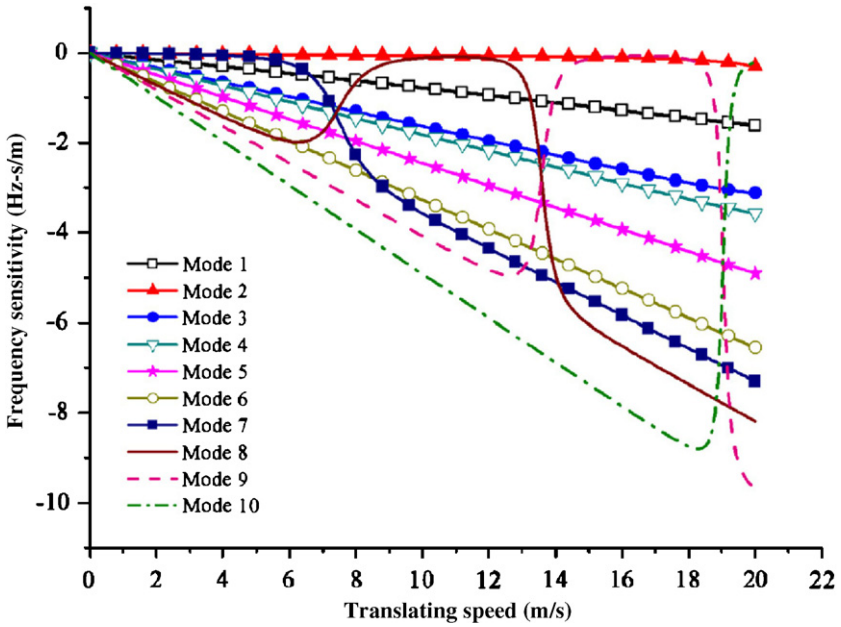

Fig. 10. Sensitivity of the first 10 frequencies with respect to belt speed c.

transverse vibration dominated modes have negative sensitivity that is basically proportional to the reciprocal of the speed. These agree with widely accepted understanding that the frequency of a transverse vibration of the belt decreases when the belt speed increases. In addition, it can be found that the frequencies of modes 8–10 vary abruptly at some speeds. The phenomenon reveals mode transfer at these speeds, or more exactly, a transverse vibration dominated mode changes to a rotational vibration dominated mode, or vice versa.

6.2. Optimization for vibration reduction

An accessory belt drive of a 6-cylinder engine [9] shown in Fig. 11 is used to exemplify the aforementioned optimal algorithm. The parameters of the system are listed in Table 2.

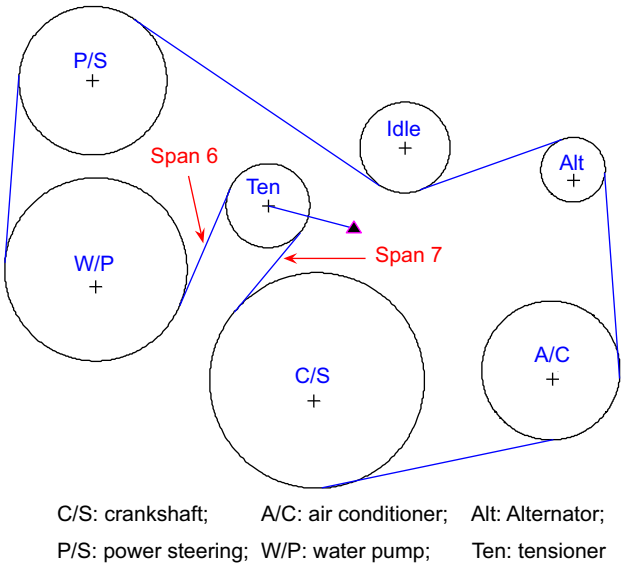

Fig. 11. Configuration of a belt drive of multiple pulleys.

Table 2
Parameters of a belt drive of multiple pulleys

Component	(x, y)[a](m)	r_i/L (m)	J_i/J_t (kg m^2)
C/S	(0,0)	0.097	0.122
A/C	(0.2116,0.009)	0.0625	0.003785
Alt	(0.2317,0.1898)	0.0291	0.0043
Idle	(0.0796,0.2097)	0.04075	0.00024
P/S	(−0.2026,0.2699)	0.06685	0.000596
W/P	(−0.2,0.1)	0.08245	0.004596
Ten	(−0.0443,0.15745)[b]	0.03775	0.000043
Tensioner arm	(0.033, 0.137)	0.08	0.004601
Other parameters	Belt: EA = 111,200 N; $m = 0.107$ kg/m; $P_{0i} = 257$ N Tensioner: $k_r = 38.84$ N · m/rad; $\theta_a = 165.25°$		

[a](x, y) are the coordinates of a pulley center or the tensioner arm pivot. Center coordinates of tensioner pulley are calculated according to θ_a and L.
[b]The underlined values are the initial ones for those to be optimized.

Free vibration analysis reveals that the first rotationally dominated mode of the belt drive has a frequency of $\omega_1^r = 39.9$ Hz. Assume that the idle speed of that engine is 800 rev/min, and that an excitation occurs to the crankshaft when the engine is at idling status. The exciting frequency can be assumed as $\omega_e = k\omega_0$ with

$\omega_0 = 40\,\text{Hz}$ and $k = 1,2,\ldots$. At the idling speed, it is derived that $c = 8.1263\,\text{m/s}$. For a linear system, the amplitude of any component under steady vibration to a harmonic excitation is proportional to the force amplitude A_f. For simplicity but without loss of generality, it is further assumed that $\omega_e = \omega_0$ and $A_f = 10\,\text{N m}$.

It is clear that resonance happens to the belt drive due to such an excitation, as the frequency ω_e is very close to the first rotational frequency ω_1^r. Optimal design will be conducted to reduce the vibration of all components as much as possible.

As mentioned before, the design variables are parameters relative to the tensioner, i.e. θ_a, L and k_r. The objective function is defined in Eq. (33) with $\mu_i = \mu_t = \mu_{b1} = \mu_{b2} = 1$ for simplicity. Geometrical analysis to avoid motion interference and a simple consideration about the possible stiffness of the torsional spring lead to the following constraints:

$$\begin{cases} 150 \leqslant \theta_a \leqslant 180, \\ 0.07 \leqslant L \leqslant 0.11, \\ 10 \leqslant k_r \leqslant 100. \end{cases} \tag{38}$$

Units of the design variables are degree (°), meter (m) and N m/rad, respectively. It should be noted that requirement on the take-up ratio of the tensioner has not been considered during choosing the boundaries of k_r.

The values of the design variables resulted from optimization are $\theta_a = 177°$, $L = 0.07\,\text{m}$, $k_r = 10\,\text{N m/rad}$, which render the first rotational frequency to be $\omega_1^r = 38.6\,\text{Hz}$. The amplitudes of all components before and after optimization are presented in Table 3, while the time histories of the responses are plotted in Figs. 12–17.

Table 3
Amplitudes of components before/after optimization

Components	C/S	A/C	Alt	Idle	P/S	W/P	Ten	Arm	Span 6	Span 7
A_i^{origin} (mm)	7.94	4.67	15.0	17.0	20.5	22.4	6.62	16.3	4.27	14.7
A_i^{new} (mm)	0.606	0.222	0.909	1.08	1.38	1.55	0.305	1.46	1.16	3.95

Note: (1) A_i^{origin} represents amplitude of the prototype system while A_i^{new} is amplitude of the system with optimized parameters.
(2) Amplitudes of both belt spans are defined by Eq. (19).

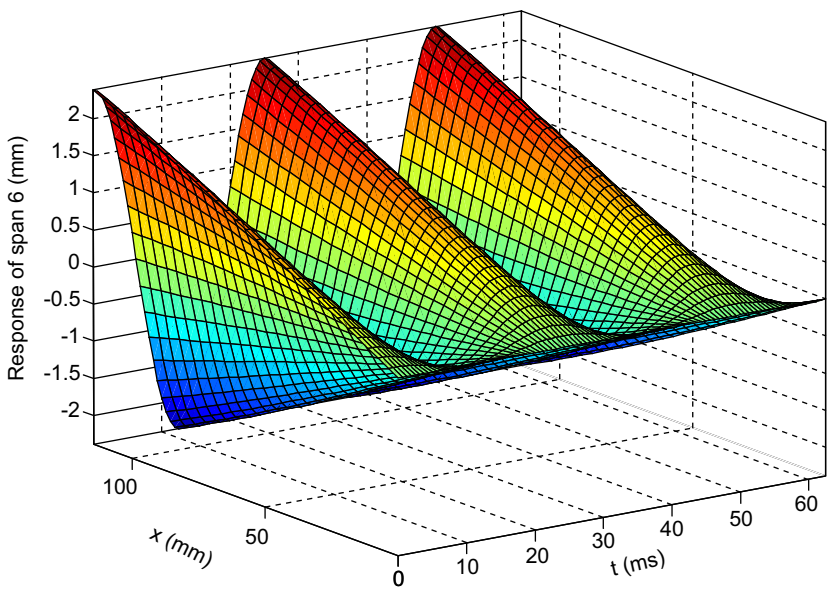

Fig. 12. Response of belt span 6 before optimization.

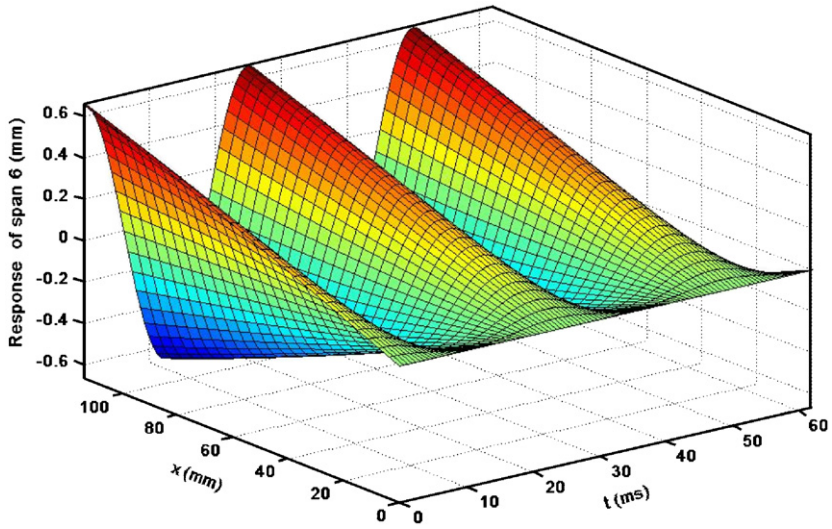

Fig. 13. Response of belt span 6 after optimization.

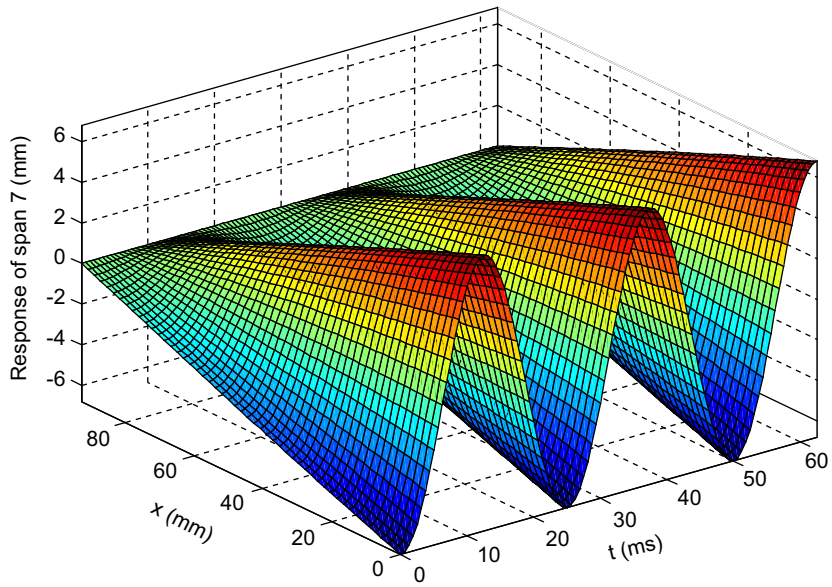

Fig. 14. Response of belt span 7 before optimization.

Before discussion, it has to be pointed out that the amplitudes of the belt spans in Table 3 are smaller than the real maximum values of the dynamic responses of either belt span. This discrepancy comes from the definition of the amplitude given in Eq. (19), which is adopted for simplicity.

Table 3 and the figures clearly show that by optimization the vibration amplitudes of all components are dramatically reduced. The reason lies in frequency detuning. The frequency of the first rotationally dominated mode of the new belt drive, $\omega_1^r = 38.6\,\text{Hz}$, is away from the exciting frequency $\omega_e = 40\,\text{Hz}$ compared with $\omega_1^r = 39.9\,\text{Hz}$ of the original drive. Further analysis reveals that 38.6 and 40.6 Hz are, respectively, the minimal and maximal values of the first rotational frequency under the constraint of Eq. (38). It can also be observed that the belt drive corresponding to $\omega_1^r = 40.6\,\text{Hz}$ has a higher amplitude than the system with $\omega_1^r = 38.6\,\text{Hz}$.

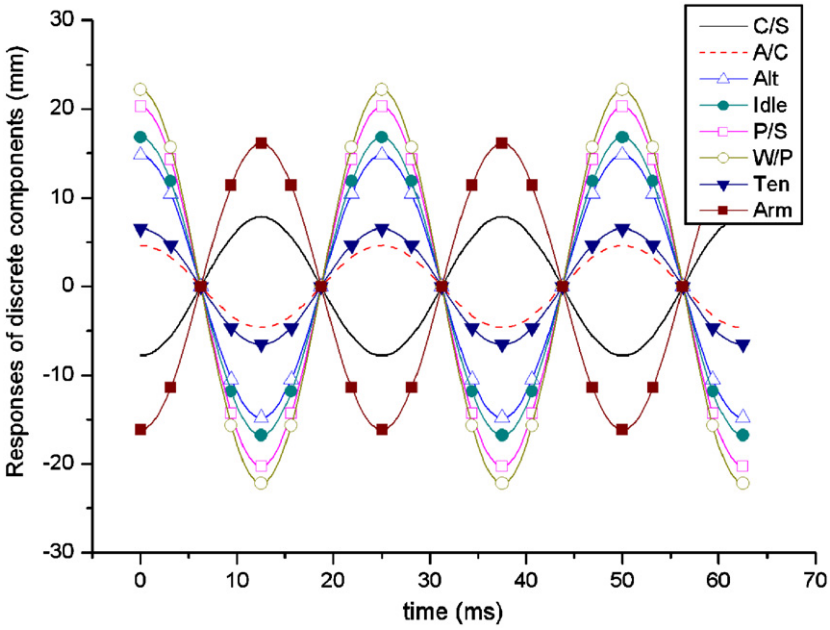

Fig. 16. Responses of discrete components before optimization.

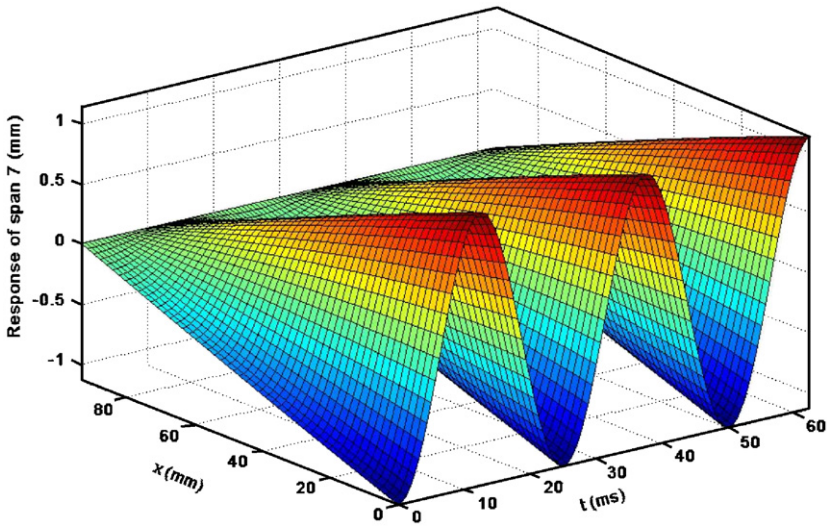

Fig. 15. Response of belt span 7 after optimization.

7. Summary

The contributions of this paper are as follows:

(1) Based on a matrix-formed equation of free vibration of the hybrid subsystem within an undamped multi-ribbed belt drive, the influence of any design parameter on natural frequencies of the subsystem is revealed by an explicit formula of frequency sensitivity with respect to the parameter. From this formula, analytical expressions are, respectively, deduced on the sensitivity of the frequencies with respect to the belt speed, the length of the tensioner arm and the installation angle of the arm.

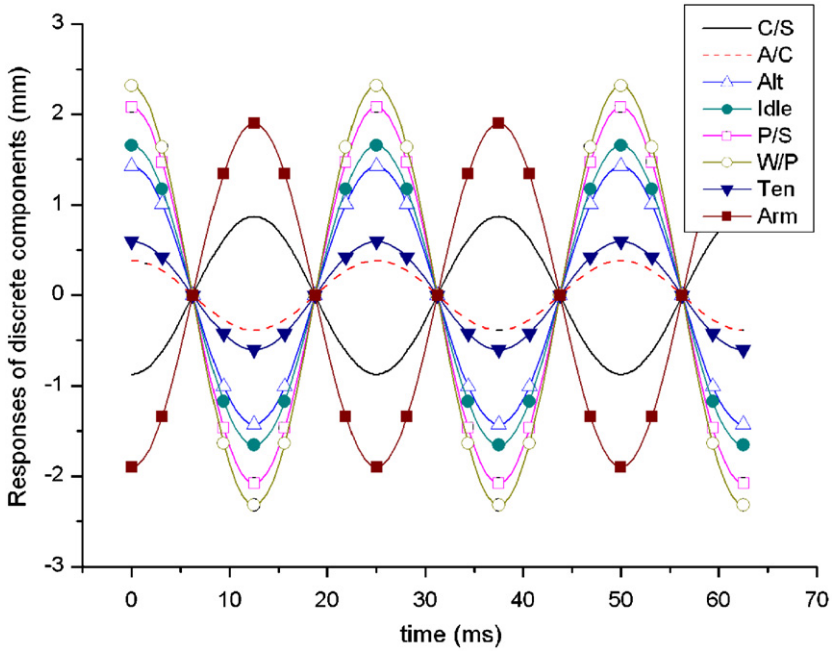

Fig. 17. Responses of discrete components after optimization.

(2) The sensitivity of the steady responses of components of the hybrid subsystem subjected to harmonic excitation is derived with respect to any design parameter.
(3) An optimization approach is put forward by combining sensitivity analysis and an ICA procedure.
(4) Given examples validate the explicit formulae of the frequency sensitivity, and demonstrate the performance of the optimization for vibration reduction.

References

[1] C.R. Barker, L.R. Oliver, W.F. Breig, Dynamic analysis of belt drive tension forces during rapid engine acceleration, SAE Paper No. 910687, 1991.
[2] S.J. Hwang, N.C. Perkins, A.G. Ulsoy, et al., Rotational response and slip prediction of serpentine belt drive systems, *Journal of Vibration and Acoustics—Transactions of the ASME* 116 (1) (1994) 71–78.
[3] S. Abrate, Vibrations of belts and belt drives, *Mechanism and Machine Theory* 27 (6) (1992) 645–659.
[4] A.G. Ulsoy, J.E. Whitsell, M.D. Hooven, Design of belt-tensioner systems for dynamic stability, *Journal of Vibrations, Acoustics, Stress, and Reliability in Design—Transactions of the ASME* 107 (3) (1985) 282–290.
[5] Fujii Atsuo, Yonemoto Shougo, Analysis of the accessory belt lateral vibration in automotive engines, *JSAE Review* 23 (2002) 41–47.
[6] R.S. Beikmann, N.C. Perkins, A.G. Ulsoy, Free vibration of serpentine belt drive systems, *Journal of Vibration and Acoustics* 118 (3) (1996) 406–413.
[7] L. Zhang, J.W. Zu, Modal analysis of serpentine belt drive systems, *Journal of Vibration and Acoustics* 222 (2) (1999) 259–279.
[8] Y.X. Lao, Z.C. Hou, Z.H. Lü, Frequency sensitivity analysis on belt drive system for front end accessories of engine, *Chinese Journal of Automotive Engineering* 28 (5) (2006) 477–481.
[9] R.G. Parker, Efficient eigensolution, dynamic response, and eigensensitivity of serpentine belt drives, *Journal of Sound and Vibration* 270 (2004) 15–38.
[10] Y.X. Lao, Dynamic Analysis and Design Optimization on Front-end Accessory Belt Drives, Master Thesis, Tsinghua University, Beijing, China, 2006 (in Chinese).
[11] R.A. Sack, Transverse oscillations in traveling strings, *British Journal of Applied Physics* 5 (6) (1954) 224–226.
[12] J.A. Wickert, C.D. Mote Jr., Classical vibration analysis of axially moving continua, *Journal of Applied Mechanics—Transactions of the ASME* 57 (3) (1990) 738–744.